Available online at www.sciencedirect.com
ScienceDirect
Journal of Power Sources 160 (2006) 977–986
JOURNAL OF POWER SOURCES
www.elsevier.com/locate/jpowsour

Investigation of thermal and electrochemical degradation of fuel cell catalysts

Mei Cai [a,*], Martin S. Ruthkosky [a], Belabbes Merzougui [b], Swathy Swathirajan [c], Michael P. Balogh [a], Se H. Oh [a]

[a] *General Motors Research and Development Center, United States*
[b] *Aerotek, United States*
[c] *General Motors Fuel Cell Activities, United States*

Received 9 February 2006; received in revised form 10 March 2006; accepted 10 March 2006
Available online 11 May 2006

Abstract

A significant problem hindering large-scale implementation of proton exchange membrane (PEM) fuel cell technology is the loss of performance during extended operation and automotive cycling. Recent investigations of the deterioration of cell performance have revealed that a considerable part of the performance loss is due to the degradation of the electrocatalyst. In this study, an attempt is made to experimentally simulate the degradation processes such as carbon corrosion and platinum (Pt) surface area loss using an accelerated thermal sintering protocol. Two types of Tanaka fuel cell catalyst samples were heat-treated at 250 °C in humidified helium (He) gas streams and several oxygen (O_2) concentrations. The catalysts were then cycled electrochemically in pellet electrodes to determine the hydrogen adsorption (HAD) area and its evolution in subsequent electrochemical cycling. Samples that had undergone different degrees of carbon corrosion and Pt sintering were characterized for changes in carbon mass, active Pt surface area, BET (Brunauer, Emmett and Teller) surface area, and Pt crystallite size. Studies of the effect of oxygen and water concentration on two Tanaka catalysts, dispersed on carbon supports with varying BET areas, revealed that carbon oxidation in the presence of Pt follows two pathways: an oxygen pathway that leads to mass loss due to formation of gaseous products, and a water pathway that results in mass gains, especially for high BET area supports. These processes may be assisted by the formation of highly reactive OH and OOH type radicals. Platinum surface area loss, measured at varying oxygen concentrations and as a function of sintering time using X-ray diffraction (XRD), CO chemisorption, and electrochemical hydrogen adsorption, reveal an important role for carbon corrosion rather than an increase in Pt particle size for the surface area loss. Platinum surface area loss during 10 h of thermal degradation was equivalent to electrochemical degradation observed over 500 cycles for a Tanaka Pt/Vulcan electrode cycled between 0 and 1.2 V (normal hydrogen electrode-NHE). Carbon mass loss observed for 5 h of thermal degradation was comparable to that obtained during a potential hold for 86 h at 1.2 V (NHE) and 95 °C for the same catalysts.

Keywords: Electrocatalyst; Carbon corrosion; PEM fuel cell; Degradation mechanism; Thermal oxidation

1. Introduction

Proton exchange membrane (PEM) fuel cells have been intensively developed in recent years as an alternative power source for stationary and mobile applications. Automotive packaging has been demonstrated due to the high power density of PEM fuel cell stacks, but widespread commercialization has made little progress due to durability and cost issues. PEM fuel cells use electrocatalysts for the oxidation of hydrogen at the anode and reduction of oxygen in air at the cathode. Currently, platinum (Pt) or platinum alloys supported on high surface area carbons is the only feasible electrocatalyst for PEM fuel cell systems [1]. In order to obtain optimized catalytic activity and reduce overall system cost, Pt is generally dispersed as nano-sized particulates. High surface area carbons are used as supports to disperse nano-sized Pt, allow facile mass transport of reactants and products of the fuel cell reactions, and to provide good electrical conductivity. Any deterioration in the desired properties of platinum nanoparticles and carbon support can strongly influence the performance of PEM fuel cells [2]. It has been realized recently [3] that a significant problem hindering the large-scale implementation of PEM fuel cell technology is the

* Corresponding author. Tel.: +1 586 596 4392; fax: +1 586 986 1910.
E-mail address: mei.cai@gm.com (M. Cai).

0378-7753/$ – see front matter © 2006 Elsevier B.V. All rights reserved.
doi:10.1016/j.jpowsour.2006.03.033

loss of performance during extended operation and automotive cycling. Recent investigations on the deterioration of cell performance have revealed that a considerable part of the performance loss is due to the degradation of the electrocatalyst [4–8]. Degradation mechanisms proposed include Pt particle sintering [9], Pt dissolution [10,11], and carbon corrosion [12]. In this study, investigations are focused on carbon corrosion and Pt surface area loss. High surface area carbon supports in PEM fuel cell electrodes are exposed to corrosive conditions, which include high water exposure, low pH (<1), high temperature (50–90 °C), high potential (0.6–1.2 V), and high oxygen concentrations [12]. Moreover, the presence of Pt has been found to accelerate the rate of carbon corrosion [13,14]. During the operation of PEM fuel cells, carbon can react with some transient oxygen radicals, such as HO and HOO radicals [15], generated by the catalyst and/or water to form oxygen functionalities (e.g., lactones, ketones, alcohols, carboxylic group, etc. [16]) which then proceed to form gaseous products, CO and CO_2. In this type of degradation, the weight of carbon in catalyst layer will gradually decrease over time. As a result of carbon support loss, nano-sized Pt particles may agglomerate to form larger particles, which will lead to loss of active Pt surface area as measured by hydrogen adsorption (HAD). Since carbon corrosion occurs very slowly at potentials below 1.0 V, it is very difficult to determine its corrosion rate during active fuel cell operation. In this study, we have investigated the high temperature oxidation behavior of fuel cell catalysts to provide an experimental simulation of the degradation processes in a fuel cell. Samples that had undergone different degrees of carbon corrosion and Pt sintering were characterized for changes in carbon mass, active Pt surface area, BET (Brunauer, Emmett and Teller) surface area, and Pt crystallite size. This has also led to the development of an accelerated thermal degradation method to screen the durability of fuel cell catalysts. Also, samples heat-treated for various lengths of time have been cycled electrochemically in pellet electrodes to determine the HAD area and its evolution in subsequent electrochemical cycling. This study will enable the determination of the effect of thermal treatment and the consequent accelerated carbon corrosion and Pt sintering on the HAD area of Pt catalyst. This will also help correlate the accelerated HAD area loss due to thermal treatment to that observed during electrochemical cycling.

2. Experimental

2.1. HAD area determination with pellet electrodes

Platinized carbon powder material (Tanaka Kikinzoku Kougyo Co. Ltd. (TKK) Pt/Vulcan XC-72) that was heat treated at 250 °C in 0.7% oxygen and 8% water for 0–30 h was used to make pellet electrodes for HAD area measurements. The platinized material was mixed with 2% polytetrafluoroethylene (PTFE) suspension and a paste was obtained by thoroughly mixing with *t*-butanol/water mixture. This paste was then pressed into a pellet using a pellet press with a current collector (Pt–Rh wire or Au gauze) incorporated in the pellet. To improve handling, the pellet was encapsulated in a polypropylene screen. It was then dried overnight under vacuum at 80 °C to remove residual alcohol. The pellet electrode was then placed in a three-electrode electrochemical cell with a Pt counter electrode and a H_2/Pt reference electrode. Cyclic voltammetric experiments were carried out in 0.5 M perchloric acid (GFS Chemicals, Inc., Ohio, USA) in argon atmosphere and 25 °C at a potential scan rate of 2 mV s^{-1}. HAD area was measured from the charge under the hydrogen adsorption peaks at 10 cycle intervals for about 100 cycles between 0 and 1.2 V (NHE).

2.2. Determination of thermal sintering conditions

Temperature programmed oxidation (TPO) was used to establish the test conditions for accelerated measurements of carbon corrosion and Pt surface area loss over a relatively short 30 h time frame. This TPO study was conducted on TKK Pt–Vulcan samples (Lot # 102-1551) for the following conditions: (1) helium (He) only, (2) 8% H_2O in He, (3) 0.7% O_2 in He and (4) 0.7% O_2 + 8% H_2O in He. The gas streams were passed through the samples while they were heated from 35 to 1000 °C at 10 °C min^{-1}. The sample effluent was monitored for key combustion/degradation components, such as CO, CO_2, O_2 and H_2O, using a mass selective detector. Fig. 1(a)–(d) shows the TPO results for the (1), (2), (3), and (4) environments above, respectively. Fig. 1(a) is a background scan, which shows an initial increase in CO, CO_2 and water, peaking just before 250 °C. Since there was no O_2 present in this gas stream, the increase is likely due to the reaction of carbon with oxygen containing functional groups on the carbon surface. Once these surface groups are depleted, the CO and CO_2 return to background levels. While Fig. 1(b) and (c) represents the effect of 8% H_2O only and 0.7% O_2 only, Fig. 1(d) reflects the combined effect of 8% H_2O and 0.7% O_2. The results show the effect of the humidified 0.7% O_2 stream with the ignition of the carbon occurring at 290 °C. When the carbon is totally consumed, O_2 returns to its initial concentration along with a corresponding drop in CO and CO_2 levels. This study enabled the selection of the following conditions for the accelerated thermal degradation experiments: gas stream oxygen concentrations of 0.7%, 0.05%, 0.004%, and 0%; moisture contents of 0% and 8%; and the temperature was chosen as 250 °C, which is below the carbon ignition point of 290 °C but high enough to provide significant carbon degradation over 30 h.

2.3. Accelerated thermal sintering

Two TKK catalysts were used for this study. TKK Pt/Vulcan (Lot # 102-1551) containing 46.6% Pt (w/w) supported on Vulcan XC-72 carbon, and TKK Pt/HSC (Lot # 102-0911) containing 45.9% Pt (w/w) supported on high surface area carbon (HSC).

BET surface area and pore size measurements were determined for fresh catalyst samples using a Micromeritics Model 2010 accelerated surface area and porosimetry system (ASAP). Sample pretreatment was especially critical for micropore determinations. Nominal sample sizes of 100 mg were initially degassed by heating under vacuum at 100 °C overnight followed

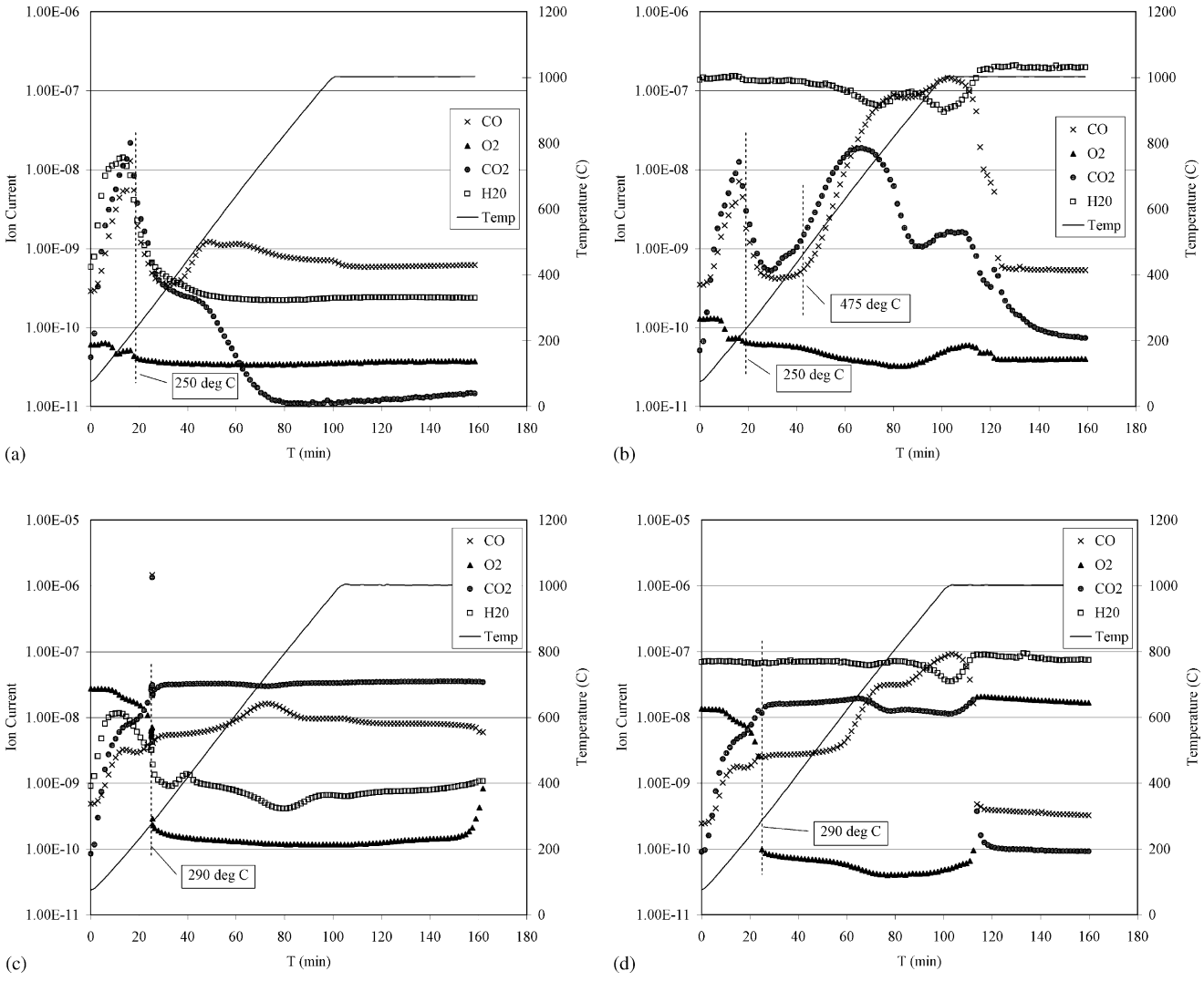

Fig. 1. (a) TPO study, He only; (b) TPO study, He + 8% H_2O; (c) TPO study, He + 0.7% O_2; (d) TPO study, He + 8% H_2O + 0.7% O_2.

by 2 h at 200 °C. The samples were tared and placed on the analysis port. Prior to analysis, the samples were heated to 200 °C for an additional 2 h under vacuum. Mesopore volumes (20–500 Å) were determined using the BJH (Barrett, Joyner and Halenda) method and micropore (<20 Å) measurements were based on the Horvath–Kawazoe model.

Thermal sintering tests were conducted on a Micromeritics 2910 Automated Catalyst Characterization System that was modified to allow external gas inputs (H_2O, O_2 He) through the vapor accessory valve (Scheme 1). For each of the sintering periods, fresh 60 mg catalyst samples from the same batch were loaded into 2910 analysis tubes and sintered for different periods, from 0 to 30 h. Accelerated thermal sintering experiments were carried out at 250 °C in humidified He gas streams under several O_2 concentrations shown above. The total gas flow during each sintering test was held constant at 50 sccm.

Immediately following the sintering step, the external gas supply was switched off and the active catalytic (Pt) surface area of the sample was measured using pulsed CO chemisorption using the same Micromeritics Model 2910 Catalyst Characterization System. Both the sintering and analysis steps were incorporated into the 2910 method thereby allowing the sample to remain in the analysis tube for the entire process. The "sintered" sample was initially dried at 100 °C for 30 min and subsequently reduced for 30 min at 100 °C under 10% H_2 in Ar. Measured doses of the 10% CO in He analysis gas were passed through the sample where the CO chemically adsorbed on the active catalyst sites. The active metal surface area (SA, $m^2\,g^{-1}$ Pt) was calculated from the CO uptake based on a 1:1 stoichiometry between adsorbed CO and surface Pt atom. After the analysis the sample was removed and the final sample mass was recorded to determine the percent weight loss.

Samples sintered and analyzed on the Micromeritics 2910 were subsequently characterized using XRD to determine Pt crystallite size. X-ray diffraction (XRD) data were collected from 10° to 90° (2Θ angles) at $0.04°\,step^{-1}$ and $4\,s\,step^{-1}$ using Cu Kα radiation. Crystallite sizes were calculated using the Scherrer equation and the full width at half the maximum (FWHM) intensity of the Pt (2 2 0) reflection. The FWHM was calculated with peak profiling software using a pseudo-Voigt peak profile shape function.

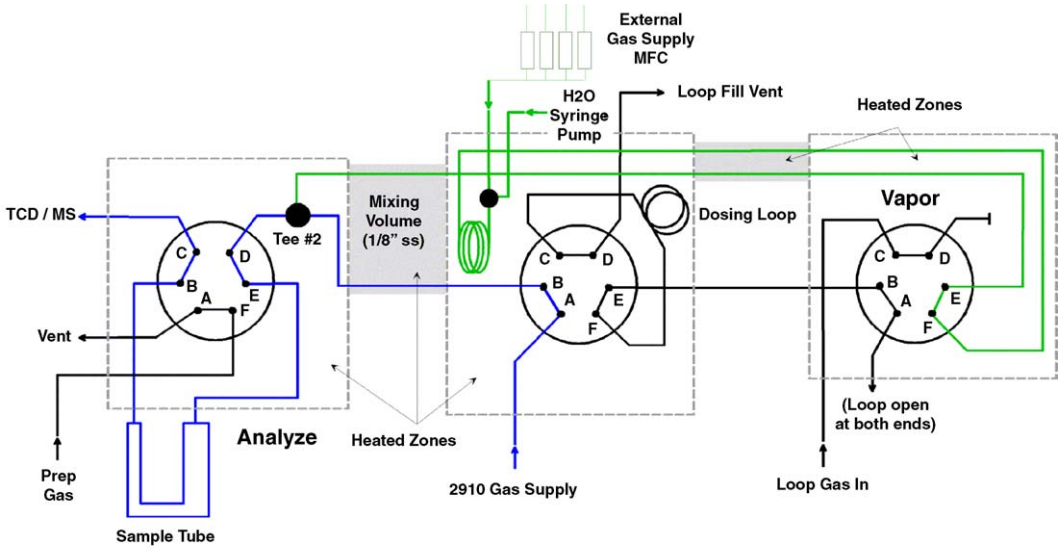

Scheme 1. Accelerated thermal sintering apparatus.

3. Results and discussion

3.1. Effect of oxygen concentration

The effect of oxygen concentration on the high temperature degradation of TKK Pt/Vulcan sample (Lot # 102-1551) was studied at 250 °C for 30 h in humidified (0% and 8% H_2O) He gas streams for O_2 concentrations of 0.7%, 0.05%, 0.004%, and 0.0%. Fig. 2 shows the carbon weight changes observed during these experiments. After 20 h of thermal treatment, the sample lost 52%, 12%, 4% and 0% of the initial carbon weight at O_2 concentration levels of 0.7%, 0.05%, 0.004% and 0%, respectively. Thus, oxygen concentration has a strong influence on the carbon corrosion rate of TKK Pt/Vulcan. Also, as discussed below, higher carbon corrosion rates lead to severe Pt surface area loss.

Fig. 3 shows changes in the active Pt surface area, as determined by pulsed CO chemisorption, observed during the same thermal aging experiments discussed in Fig. 2. Except in the case of 0.7% O_2, about a 20% increase in Pt surface area was observed after the first 4 h of treatment under all other conditions. The enhancement in Pt active surface area for the samples treated at the <0.05% oxygen indicates that oxygen helps to remove impurities adsorbed from carbon onto Pt. This behavior is also observed during electrochemical cycling in the presence of oxygen, where Pt gets quickly activated (5–10 cycles). However, cycling in argon requires at least 20 cycles to get the peak HAD area. After the initial 4 h period, the measured Pt surface area decreases with time. After 30 h of thermal treatment, the Pt surface area decreased by 70% in the 0.7% O_2 content environment while only a 4% Pt surface area loss from the initial value (41.9 $m^2\ g^{-1}$ Pt) was observed at 0.05% O_2. The results also show that Pt sintering is strongly suppressed in the absence of O_2 in the gas phase. Thus, the O_2 content in gaseous aging environment has a key role in determining the rates of both Pt sintering and carbon corrosion, and the extent of Pt sintering is related to the amount of carbon corrosion.

The thermal oxidation of carbon due to reaction with oxygen and water can follow different mechanisms in the presence and

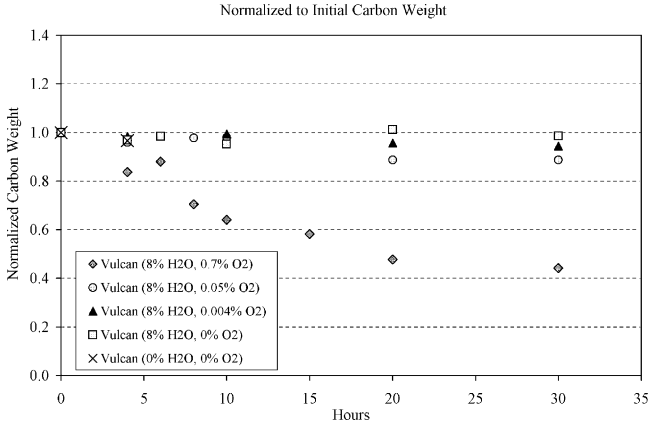

Fig. 2. Comparison of carbon corrosion rate of TKK Pt/Vulcan during thermal treatment at 250 °C in different gaseous environments.

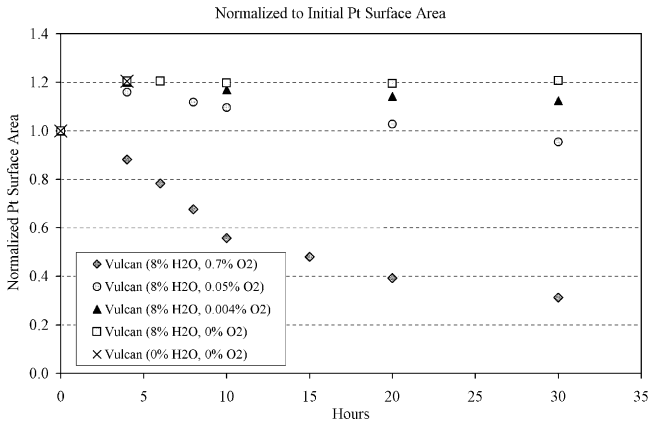

Fig. 3. Comparison of changes in the Pt surface area of TKK Pt/Vulcan during thermal treatment at 250 °C in different gaseous environments.

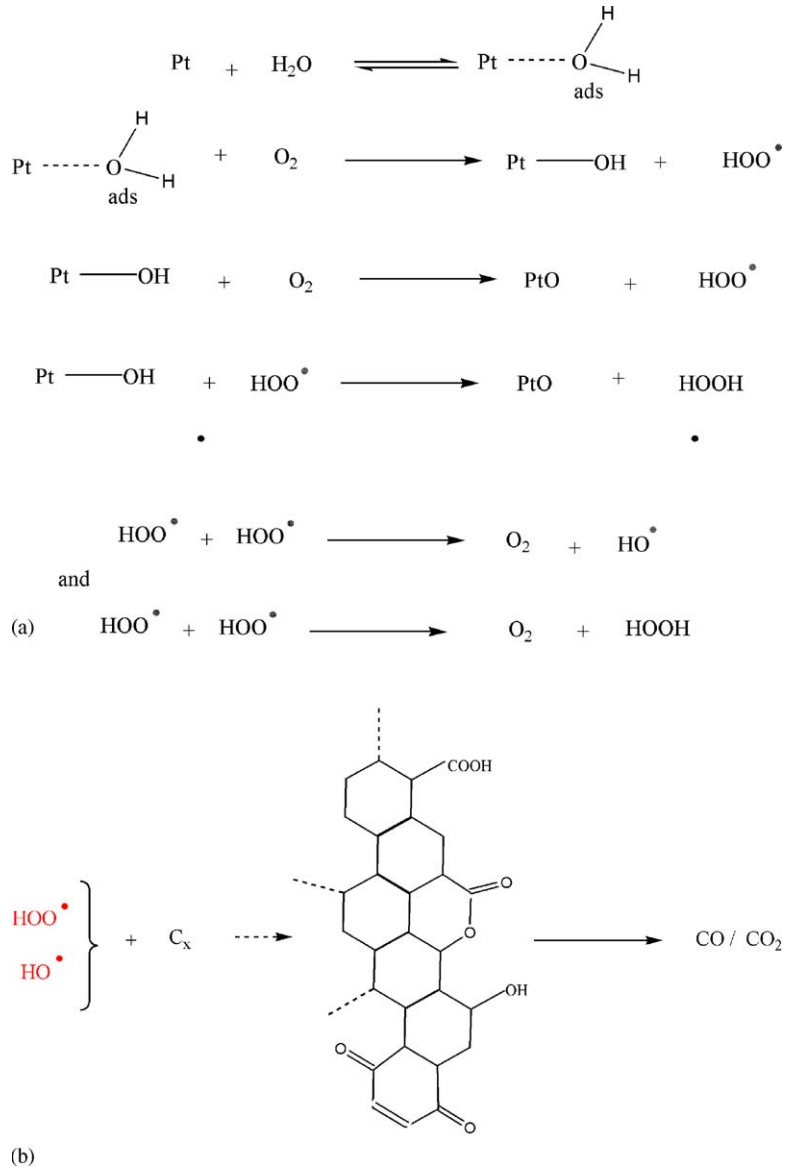

Scheme 2. (a) Formation of radicals by reaction of Pt, O_2, and H_2O; (b) carbon corrosion in the presence of Pt, O_2 and H_2O.

the absence of Pt. In the presence of Pt, Scheme 2(a) shows that Pt can react with oxygen and water to form highly reactive OH and OOH radicals. These radicals can attack carbon, as shown in Scheme 2(b), to form surface oxygen groups, which can then decompose at high temperatures to form gaseous CO and CO_2. In the absence of platinum, since carbon has unpaired electrons [17], oxygen can react with carbon through formation of radicals, as described in Scheme 3.

Fig. 4 shows changes in the Pt crystallite size, as determined by XRD, of TKK Pt/Vulcan under three different thermal treatment conditions. Pt particle size nearly doubled from the initial 3.6 nm after 20 h of treatment at 250 °C in the 0.7% O_2 case. However, at oxygen concentrations of <0.05%, the increase in Pt crystallite size was less than 10%. No significant differences in Pt crystallite sizes were observed for $O_2 < 0.05\%$, which is in qualitative agreement with surface area changes shown in Fig. 3. Based on these heat treatment results, Pt particle growth and the

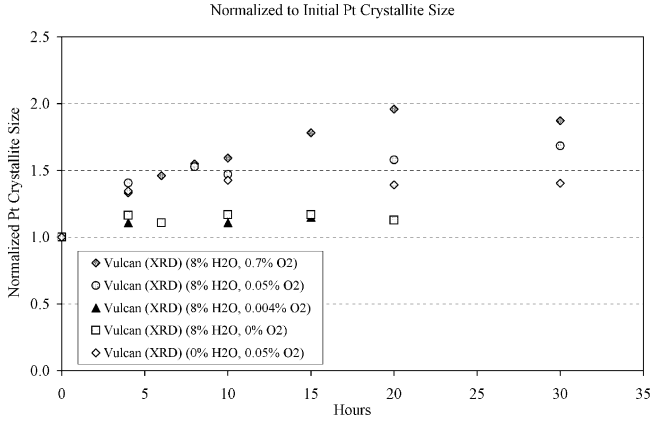

Fig. 4. Comparison of changes in Pt crystallite size of TKK Pt/Vulcan during thermal treatment at 250 °C in different gaseous environments.

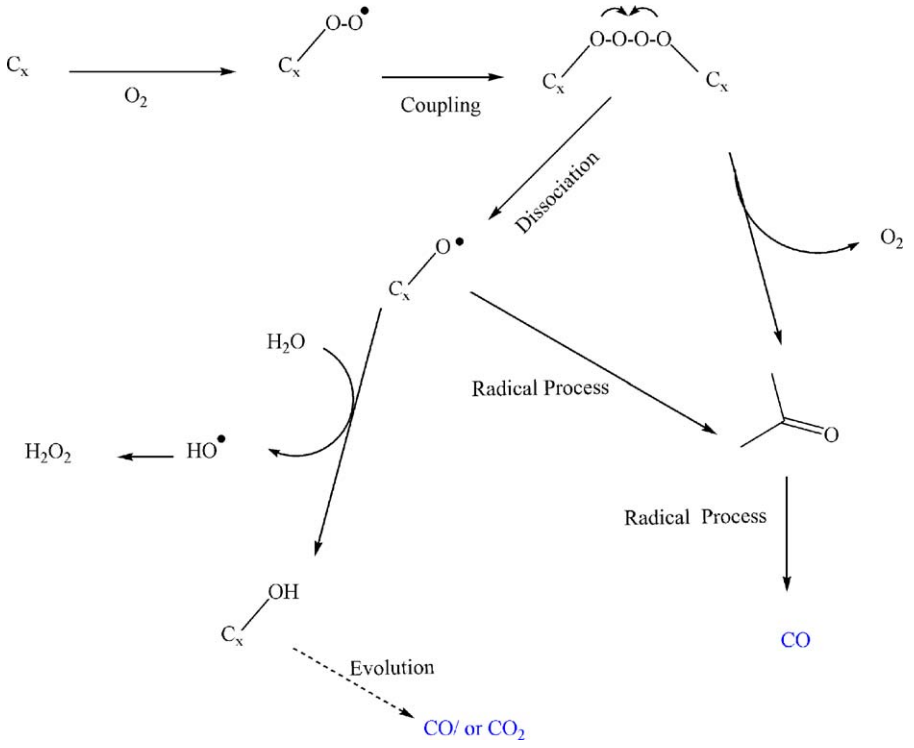

Scheme 3. Carbon corrosion in the absence of Pt.

consequent loss in its real area may be mainly induced by carbon corrosion.

3.2. Effect of carbon support

Gas phase thermal aging experiments were carried out for two TKK fuel cell catalysts dispersed on two different carbon supports to investigate the effect of carbon surface area. Table 1 lists the physical properties of the two Tanaka catalysts. The Pt content of the two catalysts is about 46% and the BET area of the platinized TKK Pt/HSC sample was a factor of four higher than the Vulcan-supported catalyst. Fig. 5 compares the carbon weight loss as a function of sintering time. At the end of the 30 h sintering period, the TKK Pt/HSC and TKK Pt/Vulcan lost 74% and 56% of their initial carbon weights, respectively. This result indicates that carbon corrosion rate is proportional to the BET surface area, though the BET area normalized rate is lower for the high surface area carbon compared to Vulcan. Electrochemical oxidation of these two catalyst samples have been studied [18] at 95 °C in 0.5 M sulfuric acid as a function of potential in the range 0.8–1.2 V (NHE). At a positive potential of 1.2 V, which could be a positive operating potential limit for a hydrogen/air fuel cell, carbon weight losses for the two catalysts over 86 h of potential hold were comparable to the carbon weight losses obtained in the current study over a 5 h period.

In order to characterize the kinetics of carbon corrosion, a power law model of the sort given by Eq. (1) was used to fit the carbon weight losses:

$$dW/dt = -kW^n \quad (1)$$

where W is the carbon weight, t the sintering time, n the order of the corrosion reaction with respect to the activity of the solid

Table 1
Physical properties of two Tanaka catalysts

	TKK Pt/Vulcan	TKK Pt/HSC
Lot #	102-1551	102-0911
Pt content (%)	46.6	45.9
BET SA ($m^2\ g^{-1}$)	105	425
Pore SA ($m^2\ g^{-1}$)	72	298
BJH mesopore volume ($cm^3\ g^{-1}$) (20–500 A)	0.24	0.62
Average pore diameter (A)	76	82
Active Pt SA ($m^2\ g^{-1}$ Pt) (CO chemisorption-as received)	41.9	71.2
Pt crystallite size (nm) (XRD)	3.6	2.6

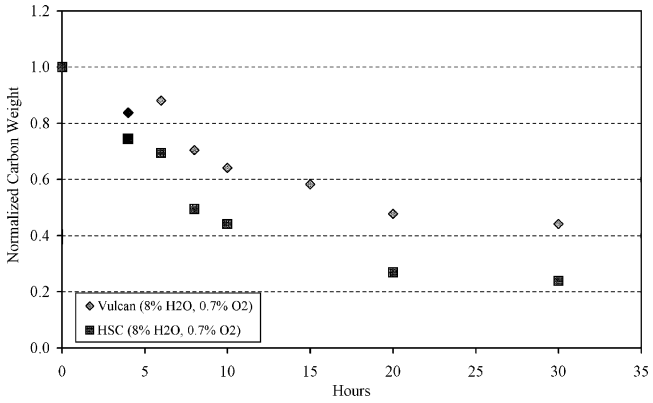

Fig. 5. Carbon weight loss for TKK Pt/HSC and TKK Pt/Vulcan catalysts during thermal treatment in 0.7% O_2–8% H_2O in He at 250 °C.

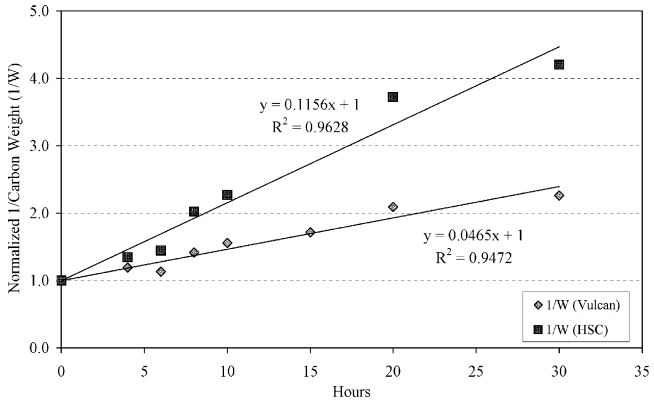

Fig. 6. Description of carbon weight loss for TKK Pt/HSC and TKK Pt/Vulcan catalysts can be described by second-order kinetics.

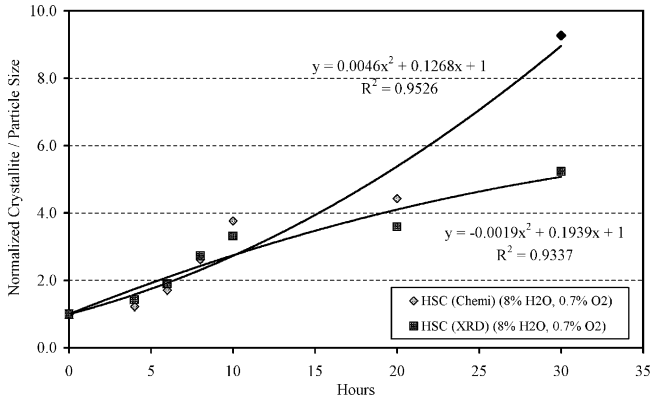

Fig. 8. Pt particle sizes as determined by CO chemisorption and XRD at various thermal sintering times for TKK Pt/HSC in 0.7% O_2–8% H_2O in He.

phase represented by the mass of the material, and k is the rate constant. Integration of Eq. (1) and noting that $W = W_0$ at $t = 0$, one obtains:

$$W = W_0 \exp(-kt), \quad n = 1 \tag{2}$$

$$(W_0/W)^{n-1} = kW_0^{n-1}(n-1)t + 1, \quad n > 1 \tag{3}$$

Best fit of the experimental data was obtained with Eq. (3) for $n = 2$, as shown in Fig. 6. The quality of the fit suggests that the measured carbon weight losses under these sintering conditions can be well described by second-order corrosion kinetics.

Fig. 7 compares the Pt particle sizes calculated from active Pt surface area determined by CO chemisorption and those determined by XRD as a function of sintering time for TKK Pt/HSC. In general, the Pt crystallite size determined by XRD was significantly smaller than that the particle size determined by CO chemisorption (2.6 nm versus 3.9 nm for the fresh unsintered Pt/HSC sample). When the estimated Pt sizes are normalized to their initial values (as displayed in Fig. 7), useful insight can be gained on the thermal sintering of Pt. Previous studies [19–22] have focused on two mechanisms for the kinetics of particle size growth, viz, particle migration and crystallite growth through Ostwald ripening. Pt particle/crystallite growth rates determined by chemisorption and XRD follow closely up to 10 h

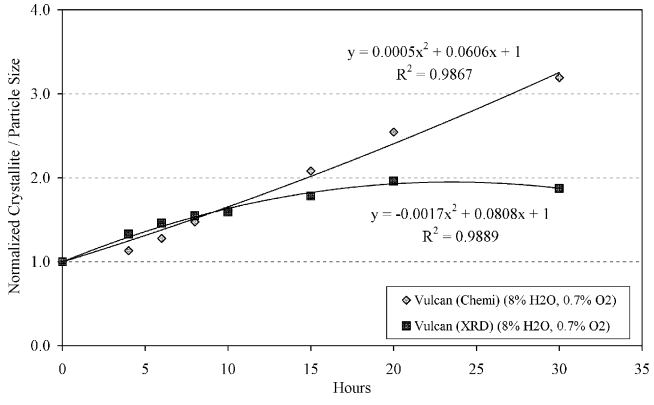

Fig. 7. Pt particle sizes as determined by CO chemisorption and XRD at various thermal sintering times for TKK Pt/Vulcan in 0.7% O_2–8% H_2O (in He atmosphere).

of sintering. However, for longer sintering times, chemisorption indicates a higher Pt particle growth rate compared to the crystallite growth rate estimated from XRD data. A similar discrepancy was observed while comparing the HAD area of TKK Pt/Vulcan and the XRD particle size as a function of potential cycling [23]. XRD particle size increased mainly in the first 15 cycles and stabilized thereafter, whereas the HAD area increased for the first 15 cycles and then continued to decay with cycling. In the first 10 h, the loss in BET may be attributed to Pt crystallite growth. After 10 h, the loss in BET may be due to the agglomeration of particles that have lost support due to carbon corrosion. A similar observation was made with TKK Pt/Vulcan, as shown in Fig. 8, although the Pt sintering rate for TKK Pt/HSC was substantially higher than that for TKK Pt/Vulcan under the same sintering conditions. This result may also be due to the smaller initial Pt particle/crystallite size for TKK Pt/HSC.

3.3. Effect of gas humidity

The effect of humidity on the high-temperature degradation of two Tanaka fuel cell catalysts (TKK Pt/Vulcan and TKK Pt/HSC) at a low O_2 concentration (0.05%) was studied at 250 °C for up to 30 h. Changes in carbon weight loss and Pt surface area (CO chemisorption) were measured at 4, 10, 20 and 30 h into the thermal sintering process, with fresh samples used for each test.

Fig. 9 shows that at the end of the 30 h thermal sintering period, the TKK Pt/Vulcan sample had lost 11% of its initial carbon mass with water present. In the absence of H_2O, however, the carbon weight loss for TKK Pt/Vulcan was only well within the measurement uncertainty. Interestingly, no significant carbon weight change was observed for TKK Pt/HSC regardless of whether or not H_2O was present in the gas stream. This is a reversal of the trend observed under the 0.7% O_2 conditions. When the oxygen concentration is <0.05%, and the surface area of carbon is much higher than the surface area of platinum, as in the case of Pt/HSC, then carbon processes to make adsorbed oxygen residues becomes more predominant in determining the overall mass changes. This may explain the mass increase for Pt/HSC. A related trend in behavior has been observed [24] from in situ quartz crystal microgravimetric (QCM) studies of carbon corro-

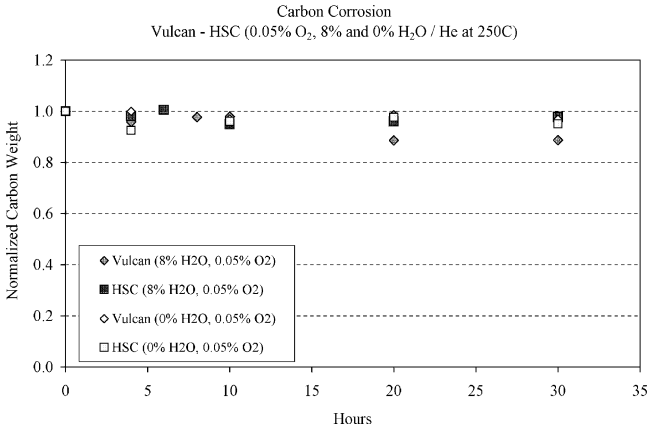

Fig. 9. Comparison of carbon corrosion rates for TKK Pt/Vulcan and TKK Pt/HSC samples sintered at 0.05% O_2 with and without H_2O.

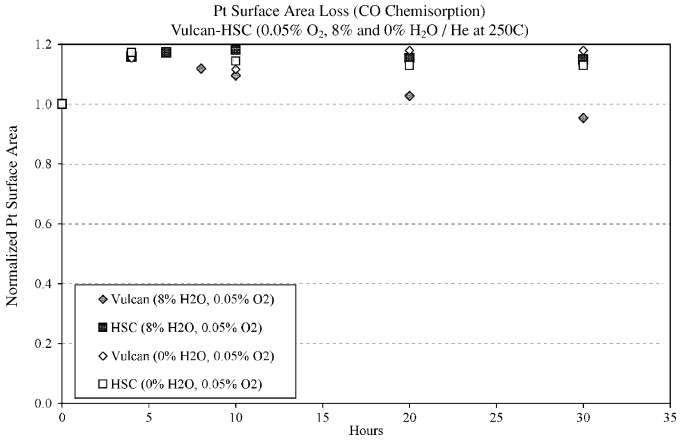

Fig. 10. Comparison of Pt surface areas, as determined by CO chemisorption, of TKK/Vulcan and TKK/HSC samples sintered at 0.05% O_2 with and without H_2O.

sion. QCM behavior at 1.2 V/NHE shows that Vulcan undergoes only weight loss with time, whereas the high surface area carbon (Black Pearls, 2000) shows an initial weight gain followed by a weight loss. Therefore, possible mechanisms include: (a) surface oxygen residue groups formed in the corrosion process stay kinetically more stable at lower O_2 concentrations; (b) two parallel corrosion paths exist that are dependent on the H_2O/O_2 ratio; (c) H_2O plays a more dominant role at lower O_2 concentrations; (d) Vulcan is active towards oxygen reduction because of the presence of enol/quinone groups, and thus more peroxide radicals are probably formed leading to more carbon corrosion as shown in Scheme 4.

Platinum surface area determined by CO chemisorption is shown in Fig. 10 for thermal sintering in the presence of 0.05% O_2. When sintered in dry feed, both the TKK Pt/HSC and TKK Pt/Vulcan samples showed no significant decrease in Pt surface area. Except the TKK Pt/Vulcan sample in a humid environment, Pt surface area increased nearly 20% after the first 4 h treatment and maintained the same level throughout the remainder of the 30 h sintering process.

3.4. Effect of thermal treatment on HAD area loss

Cyclic voltammetric behavior of the pellet electrodes made from samples aged for 0–30 h are shown in Fig. 11. The loss in HAD area is clearly observed due to thermal aging. Also, shifts in the oxide reduction, hydrogen adsorption and oxidation

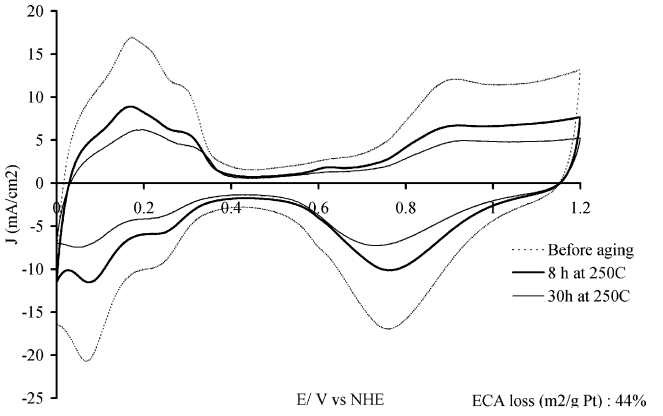

Fig. 11. Cyclic voltammetric response of TKK Pt/Vulcan (Lot 102-1551) before and after thermal aging at 250 °C, in 0.7% O_2 and 8% water. Electrolyte: 0.5 M perchloric acid; potential scan rate: 2 mV s^{-1}. Ar atmosphere and room temperature.

peaks are observed for the sample that was aged for 30 h, probably due to the oxidation of carbon support leading to higher ohmic potential drop in the electrode. A similar behavior has been noticed for Pt/HSC, cycled for 500 cycles between 0 and 1.2 V/NHE.

The evolution of HAD area with increasing number of cycling for the TKK Pt/Vulcan samples before and after heat treatment

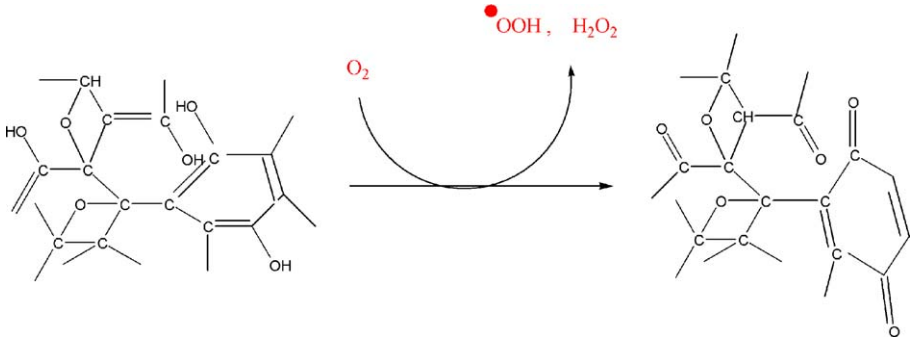

Scheme 4. Reaction of oxygen with enol groups on Vulcan carbon surface.

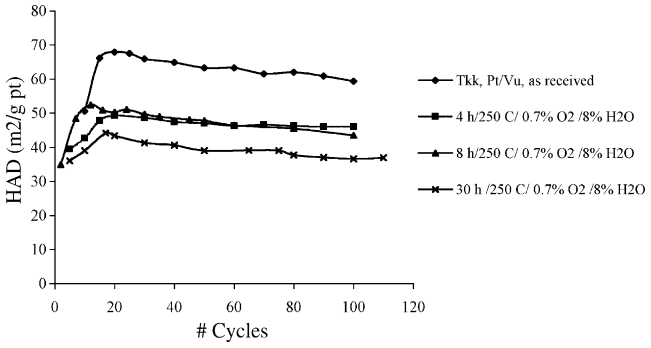

Fig. 12. Comparison of HAD areas and cycling behavior of TKK Pt/Vulcan, Lot # 102-155, heat-treated at different conditions. 2 mV s^{-1}; potential limits: 0–1.2 V/NHE; 0.5 M $HClO_4$, argon and 25 °C.

is shown in Fig. 12. Potential cycling measurements on all the thermally sintered samples show lower peak HAD areas and more stable cycling behavior. Peak HAD area losses for the sintered samples were lower than the Pt surface area loss predicted by X-ray particle size measurement, which in turn were lower than that calculated from CO chemisorption measurements. For example, HAD area losses for the 8 and 30 h sintered samples were 21% and 33%, respectively, compared to 33% and 66% from CO chemisorption data and 35% and 46% suggested by X-ray diffraction crystallite size measurements. This result can be attributed to an increase in the active area of the electrode caused by an efficient removal of adsorbed impurities during electrochemical cycling, as suggested by Bett et al. [25]. Alternatively, there may have been an increase in the hydrophilicity of the electrode due to the oxidation of the carbon support, which may cause an increase in the wettability and hence the active HAD area (enhancement in Pt utilization) of the electrode. However, the cyclic voltammetric response and HAD area of the sample heat treated for 10 h were similar to those obtained with a pellet electrode sample that had undergone 500 cycles [26] between the same potential limits. This suggests that the mechanism of surface area loss in the electrochemical environment is probably similar to the gas phase environment, and may therefore involve Pt particle size growth and carbon corrosion. Pt particle size may increase due to Pt dissolution/redeposition phenomena [27]. Carbon oxidation to gaseous species can cause agglomeration of Pt particles, leading to loss of catalyst dispersion [28,29]. The favorable correlation between HAD area loss due to cycling and thermal degradation on the one hand, and between carbon loss during potential hold and high temperature oxidation on the other, as mentioned above, all indicate that electrochemical catalyst degradation may be conveniently simulated by high temperature experiments.

4. Conclusions

1. Carbon corrosion and platinum surface area loss that are observed for electrocatalysts over long periods of electrochemical cycling and potential hold can be conveniently simulated by high temperature experiments at 250 °C in an environment containing about 0.7% oxygen, 8% water and helium (balance). Accelerated screening of catalysts is not possible at oxygen concentrations of <0.05%.
2. Platinum surface area loss during 10 h of thermal degradation was equivalent to electrochemical degradation observed over 500 cycles for a Tanaka Pt/Vulcan electrode cycled between 0 and 1.2 V (NHE). Carbon mass loss observed for 5 h of thermal degradation was comparable to the mass loss observed during a potential hold for 86 h at 1.2 V (NHE) and 95 °C for the same catalysts.
3. Studies on the effect of oxygen and water concentration on two Tanaka catalysts, dispersed on carbon supports varying in their BET areas, revealed that carbon oxidation in the presence of Pt follows two pathways: an oxygen pathway that leads to mass loss due to formation of gaseous products, and a water pathway that results in mass gains, especially for high BET area supports. These processes may be assisted by the formation of highly reactive OH and OOH radicals.
4. Platinum surface area loss, measured at varying oxygen concentrations and as a function of sintering time using X-ray diffraction, CO chemisorption and electrochemical hydrogen adsorption, reveals an important role for carbon corrosion rather than an increase in Pt particle size for the surface area loss.

Acknowledgments

The authors wish to thank Hubert Gasteiger, Frederick Wagner, Rohit Makharia, Shyam Kocha, Wei Li, Michael Carpenter, and Lee Feng for the valuable discussions during this investigation.

References

[1] P. Costamagna, S. Srinivasan, J. Power Sources 102 (2001) 242.
[2] M. Gangeri, G. Centi, A. La Malfa, S. Perathoner, R. Vieira, C. Pham-Huu, M.J. Ledoux, Catal. Today 102–103 (2005) 50–57.
[3] D.A. Stevens, J.R. Dahn, Carbon 43 (2005) 179–188.
[4] T. Tada, in: W. Vielstich, A. Lamm, H.A. Gasteiger (Eds.), Handbook of Fuel Cells, Fundamentals Technology and Applications, vol. 3, Wiley, New York, 2003, pp. 481–488.
[5] K. Mitsuda, Y. Gonjo, H. Maeda, H. Fukumoto, Proceeding of the 1998 Fuel Cell Seminar, 1998, pp. 541–544.
[6] T.E. Springer, M.S. Wilson, F. Garzon, T.A. Zawodzinski, S. Gottesfeld, Polymer Electrolyte Fuel Cells for Transportation Applications, Los Alamos National Laboratory, 1993.
[7] J. St-Pierre, D.P. Wilkinson, S. Knight, M. Bos, J. New Mater. Electrochem. Syst. 3 (2000) 99–106.
[8] E. Gulzow, H. Sander, N. Wagner, M. Lorenz, A. Schneider, M. Schulze, Proceedings of the 2000 Fuel Cell Seminar, 2000, pp. 156–160.
[9] M.S. Wilson, H.G. Garzon, K.E. Sickafus, S. Gottesfeld, J. Electrochem. Soc. 140 (10) (1993) 2872.
[10] R.M. Darling, J.P. Myers, J. Electrochem. Soc. 150 (2003) A1523.
[11] J.P. Meyers, R.M. Darling, Proceedings of the 202nd Meeting of the Electrochemical Society, 2002.
[12] L.M. Roen, C.H. Paik, T.D. Jarvi, Electrochem. Solid State Lett. 7 (1) (2004) A19–A22.
[13] K. Kinoshita, J. Bett, Carbon 12 (1974) 525.
[14] R. Makharia, P. Yu, J. Pisco, S. Kocha, H. Gasteiger, ECS Meeting, 2004.
[15] A. Panchenko, H. Dilger, J. Kerres, M. Hein, A. Ulrich, T. Kaqz, E. Roduner, Phys. Chem. Chem. Phys. 6 (2004) 2891–2894.

[16] K.H. Kangasniemi, D.A. Condit, T.D. Jarvi, J. Electrochem. Soc. 151 (4) (2004) E125–E132.
[17] A. Panchenko, H. Dilger, E. Möller, T. Sixt, E. Roduner, J. Power Sources 127 (1–2) (2004) 325–330.
[18] I. Halalay, G. Garabedian, S. Swathirajan, unpublished work.
[19] J.A. Bett, K. Kinoshita, P. Stonehart, J. Catal. 35 (1974) 307–316.
[20] J.A.S. Bett, K. Kinoshita, P. Stonehart, J. Catal. 41 (1976) 124–133.
[21] E. Ruckenstein, B. Pulvermacher, AIChE J. 19 (1973) 356.
[22] E. Ruckenstein, B. Pulvermacher, J. Catal. 29 (1973) 224.
[23] B. Merzougui, G. Nazri, S. Swathirajan, unpublished work.
[24] B. Merzougui, S. Swathirajan, unpublished work.
[25] J. Bett, K. Kinoshita, K. Routsis, P. Stonehart, J. Catal. 29 (1973) 160–168.
[26] B. Merzougui, S. Swathirajan, Proceedings of the 209th Meeting of the Electrochemical Society, 2006.
[27] K. Kinoshita, J.T. Lundquist, P. Stonehart, J. Electroanal. Chem. 48 (1973) 157.
[28] P.N. Ross, in: E.E. Petersen, A.T. Bell (Eds.), Catalyst Deactivation, Marcel Dekker, New York, 1987, pp. 165–187.
[29] L. Gmachowski, Colloids Surf. A 197 (2002) 183–191.